



**Effects of grain boundary structure and shape of the solid-liquid interface on the growth direction of the grain boundaries in multicrystalline silicon**

Journal:	<i>CrystEngComm</i>
Manuscript ID	CE-ART-11-2021-001573.R2
Article Type:	Paper
Date Submitted by the Author:	29-Jan-2022
Complete List of Authors:	Fukuda, Yusuke; Nagoya University, Engineering Kutsukake, Kentaro; RIKEN Kojima, Takuto; Nagoya University, Usami, Noritaka; Nagoya University - Higashimaya Campus, Graduate School of Engineering

SCHOLARONE™  
Manuscripts

## ARTICLE

## Effects of grain boundary structure and shape of the solid-liquid interface on the growth direction of the grain boundaries in multicrystalline silicon

Received 00th January 20xx,  
Accepted 00th January 20xx

DOI: 10.1039/x0xx00000x

Yusuke Fukuda<sup>\*a</sup>, Kentaro Kutsukake<sup>b</sup>, Takuto Kojima<sup>c</sup> and Noritaka Usami<sup>a</sup>

We report on the effects of grain boundary (GB) structure on the growth direction of the GBs by utilizing silicon ingots with artificially designed asymmetric tilt GBs. The ingots were grown by directional solidification using the seed crystal formed by combining multiple  $\langle 110 \rangle$ -oriented or  $\langle 100 \rangle$ -oriented single crystalline silicon crystals with controlled GB planes, which could offer a unique opportunity for systematic investigation of the influences of misorientation and asymmetry. We found that GBs in  $\langle 110 \rangle$ -oriented ingots grow along the seed-oriented direction, while those in  $\langle 100 \rangle$ -oriented ingots grow away from the seed-oriented direction accompanied by the introduction of the twist component. These phenomena are explained in terms of energy minimization, assuming a linear increase of the GB energy as a function of the deviation angle and its dependence on the orientation. Specifically, we revealed that GBs with shallow energy grooves such as  $\langle 100 \rangle$  tilt GBs are more likely to grow away from the seed-oriented direction than energetically stable GBs.

### Introduction

Multicrystalline materials, which are widely used for various applications, consist of many crystal grains and grain boundaries (GBs). GB is a boundary plane between adjacent crystal grains, and the properties of individual GBs are not unique since the atomic structure should depend on relative crystal orientations to form the GBs. For example, highly consistent  $\Sigma 3$  GBs have significantly lower GB energies as determined by first-principles calculations, and they are more electrically inert than small-angle GB<sup>1-7</sup>. In other words, the function and performance of multicrystalline materials can be improved by appropriately controlling the GB structures based on understanding the relationship between the GB structure and GB properties. Therefore, many attempts have been made to improve the macroscopic properties by controlling GBs in various materials<sup>8,9</sup>. For example, GB engineering to increase a fraction of low- $\Sigma$  coincidence site lattice (CSL) GBs in a type 316L austenitic stainless steel could improve the corrosion resistance in corrosive environments<sup>10,11</sup>. The control of the GB structures in  $\text{Al}_2\text{O}_3$  could also improve high-temperature creeps resistance<sup>12-14</sup>. In addition, introducing specific low- $\Sigma$  GBs in multicrystalline silicon (mc-Si) could suppress dislocation propagation<sup>15-17</sup>. As illustrated by these examples, appropriate control of GBs is beneficial to improve the overall performance of multicrystalline materials. However, the universal guideline on controlling GBs does not exist due to the diversity and complexity of GBs. Even

for a simple material such as silicon, the atomic structures and properties of GBs are available for only a limited number of GBs.

In this study, we focus on GBs in silicon. Mc-Si has great industrial value as a substrate material for solar cells, and the control of GBs is of crucial importance among various materials because of the significant influence of GBs on electrical properties<sup>18-26</sup>. Furthermore, mc-Si comprises only one element, making it easy to develop research from microscopic observation with atomic resolution to first-principles modeling<sup>27</sup>. The obtained knowledge could be a starting point to extend to other more complicated materials.

Mc-Si is grown by the directional solidification method, in which the melt solidifies in one direction from the bottom to the top in a crucible. This directional growth process determines GB structures, and the room for structural change by annealing is limited. Therefore, we need to clarify the mechanism of determining GB structures in the solidification process for the appropriate control to improve the conversion efficiency of solar cells and material yield of an mc-Si ingot.

There have been several reports on the mechanism of the GB structure determination in Si crystals grown by directional solidification. Prakash *et al.* reported that random GBs, whose energy is independent of crystallographic orientation, grow perpendicular to the solid-liquid interface during the solidification process<sup>28</sup>. Chuang *et al.* observed that when  $\Sigma 9$  GB decomposes to form  $\{112\}\Sigma 3$  GBs, faceted grooves are formed at the junction of the solid-liquid interface and the  $\{112\}\Sigma 3$  GBs, and if the growth rates of the adjacent surfaces of the grooves are the same, the GBs grow linearly along the  $\{112\}$  plane<sup>29</sup>. Kutsukake *et al.* found that the GB structure slightly deviated from  $(310)\Sigma 5$  GB changes during growth to compensate for the deviation<sup>30</sup>. As mentioned above, an understanding of GBs, in general, is essential for making polycrystalline materials more functional by appropriately utilizing

<sup>a</sup> 1 Grad. Eng. Nagoya Univ., Nagoya, Aichi, Japan

E-mail: fukuda.yusuke@d.mbox.nagoya-u.ac.jp

<sup>b</sup> AIP, RIKEN, Nihonbashi, Tokyo, Japan

<sup>c</sup> Grad. Info. Nagoya Univ., Nagoya, Aichi, Japan

GBs (GB engineering). However, these investigations have been limited to the specific crystallographic orientation relationships (random GBs and symmetric GBs with low  $\Sigma$  values) and have not been systematically investigated. Therefore, the understanding of asymmetric GBs is very important to deepen the understanding of GBs in general. Since there are many combinations compared to symmetric GBs, systematic study to clarify the growth direction of asymmetric GBs is a challenge and essential for controlling GBs.

In this paper, we report on the mechanism of determining the GBs growth direction, including asymmetric GBs during the initial stage of solidification in terms of GB structure, using systematically produced artificial GBs with precisely designed orientation.

## Experimental

### The design of grain boundaries

GBs are classified according to the axis of rotation of the adjacent grains with respect to the GB plane as follows: 1. twist GBs (the adjacent grains have the axis of rotation perpendicular to the GB plane); 2. tilt GBs (the adjacent grains have the axis of rotation parallel to the GB plane); 3. mixed GBs (the rotation axis is intermediate between perpendicular and parallel to the GB plane). The tilt GBs are categorized into two groups: symmetric tilt GBs (the rotation angles of the adjacent grains from the GB plane are equal) and asymmetric tilt GBs (the rotation angles of the adjacent grains from the GB plane are different). The coherence of the GB structure is discussed using the  $\Sigma$  values.

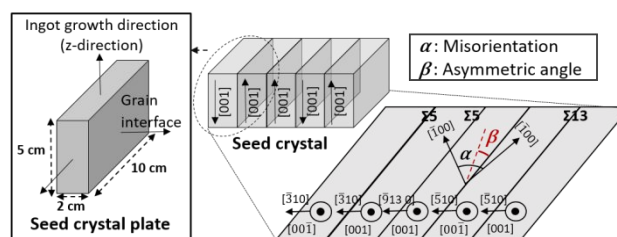


Fig. 2 Schematic diagram of seed crystal arrangement of an example of  $\langle 100 \rangle$ -designed GBs. Four GBs were fabricated by arranging the five seeds.  $\alpha$  is the misorientation between adjacent grains, and  $\beta$  is the asymmetric angle (the displacement angle of the GB plane from the symmetry plane).  $\langle 110 \rangle$ -designed GBs are also designed in the same way as  $\langle 100 \rangle$ -designed GBs.

Seed crystal plates (2 cm x 10 cm x 5 cm) used for systematic research of asymmetric GBs were cut from Czochralski grown single crystalline silicon ingots with  $\langle 100 \rangle$  and  $\langle 110 \rangle$  orientations. We designed  $\langle 100 \rangle$  and  $\langle 110 \rangle$  tilt GBs including asymmetric tilt GBs by arranging the seed crystal plates with the same crystallographic orientation in the ingot growth direction (z-direction) (Fig. 1(a)).  $\langle 100 \rangle$  or  $\langle 110 \rangle$  vertical directions are designed to be common to all crystal grains in an ingot. We also designed random GBs by using  $\langle 100 \rangle$ -oriented and  $\langle 110 \rangle$ -oriented seed crystal plates. In this way, these GBs can be expressed macroscopically in terms of three degrees of freedom: Misorientation ( $\alpha$ ) which is relative crystal orientation around z-direction, asymmetric angle ( $\beta$ ), and deviation angle from the z-direction ( $\theta$ ).

Figure 2 shows a schematic diagram of the seed crystal arrangement with  $[001]$  or  $[00\bar{1}]$  in the z-direction. Four GBs were fabricated in an ingot by arranging five seed crystal plates. As some of the GBs grow away from the z-direction,  $\langle 100 \rangle$  tilt GBs and  $\langle 110 \rangle$  tilt GBs which are designed are named  $\langle 100 \rangle$ -designed GBs and  $\langle 110 \rangle$ -designed GBs. We controlled the misorientation ( $\alpha$ ) and asymmetric angle ( $\beta$ ) of the GBs by the crystal orientation of the cut plane of the seed crystal plates. A total of twelve ingots were grown, which resulted in the formation of 47 GBs in total (one GB was

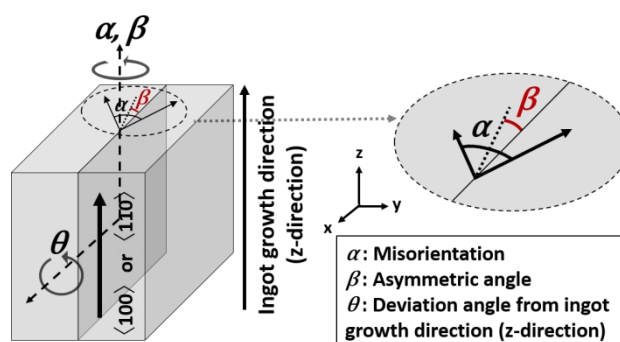


Fig. 1 The three parameters that determine the GB structure in this study (misorientation ( $\alpha$ ), asymmetric angle ( $\beta$ ), and deviation angle from z-direction ( $\theta$ )). The two small black arrows on the top surface indicate the same crystal orientation of each seed crystal such as  $[\bar{1}00]$  when z-direction is  $[001]$ .

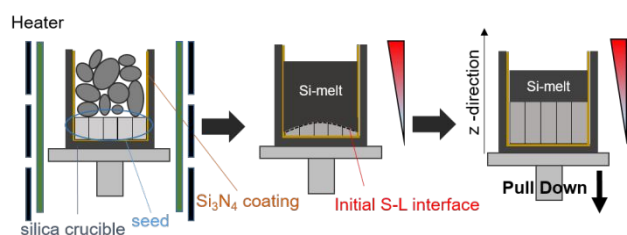


Fig. 4 Schematic diagram of crystal growth process (directional solidification method). The temperature distribution of the crystal growth furnace used in this study can be controlled by three heaters.

excluded because it split immediately at the initial of crystal growth): 17 <100>-designed GBs, 26 <110>-designed GBs, and 4 random GBs. It is noted that the number of independent designed GBs is 34 since we designed several GBs with the same  $\alpha$  and  $\beta$ .

Figure 3 shows the combination of misorientation and asymmetric angles of the GBs fabricated in this study. The colored vertical lines indicate the low  $\Sigma$  GBs. The  $\Sigma$  values of the GBs were confirmed by the electron backscatter diffraction (EBSD) method (JSM-7001F, JEOL, Inc.). Then, the measurement interval was 30  $\mu\text{m}$  and the magnification was 100x. EBSD clarified that the deviation from the designed orientation due to cutting error was  $2.4^\circ$  in average and  $5.0^\circ$  in maximum. To determine the error range of the rotation angle from the configuration of the  $\Sigma$  GBs, we used Brandon's conditional equation expressed by  $\Delta\theta = \theta_0 \Sigma^{-1/2}$ , where  $\theta_0$  is the threshold angle for  $\Sigma 1$  GB (SAGB) and we used  $15^\circ$  in this study. The <100>-designed GBs, indicated by the red dot, have an asymmetric angle in the range of 0 to  $45^\circ$  based on the four-fold symmetry of the <100> rotation axis of the silicon crystal lattice. The <110>-designed GBs, indicated by the blue triangle, have an asymmetric angle in the range of 0 to  $90^\circ$ , based on the two-fold symmetry of the <110> rotation axis of the silicon crystal lattice. The black line ( $\beta = 0$ ) corresponds to symmetric GBs. It means that only a few regions of the enormous variety have been investigated in previous studies. In addition, Figure 3 shows that systematic investigation is possible for both large and small asymmetric angles.

### Growth method

Figure 4 shows a schematic diagram of the crystal growth process of the directional solidification. The specifications of the ingots were phosphorus concentration of  $2.5 \times 10^{15} \sim 5.0 \times 10^{15} \text{ cm}^{-3}$ ,  $10 \text{ cm} \times 10 \text{ cm} \times 13 \text{ cm}$ , and 3.5 kg. The artificially designed seed crystal was placed in a quartz crucible coated with a mold release agent ( $\text{Si}_3\text{N}_4$ ) after removing the surface damage layer with HF:  $\text{HNO}_3$  (1:6) solution. The semiconductor grade Si raw materials were placed on top of the seeds. By controlling three heaters in a crystal growth furnace, all the raw materials and the top  $\sim 2 \text{ cm}$  of the seed crystal were melted. The height of the unmelted seed crystal is higher in the center. In this paper, we describe the shape of such a solid-liquid interface as convex in the growth direction, focusing on the growth front of the solid. After that, directional solidification was carried out by pulling down the crucible (0.5 mm/min), and ingots were grown while preserving the designed GBs structure<sup>31,32</sup> It is noted that the real growth rate was changing during growth, which is revealed by the results of crystal growth simulations (CGSim, STR, Inc.). The exact growth rate at each time

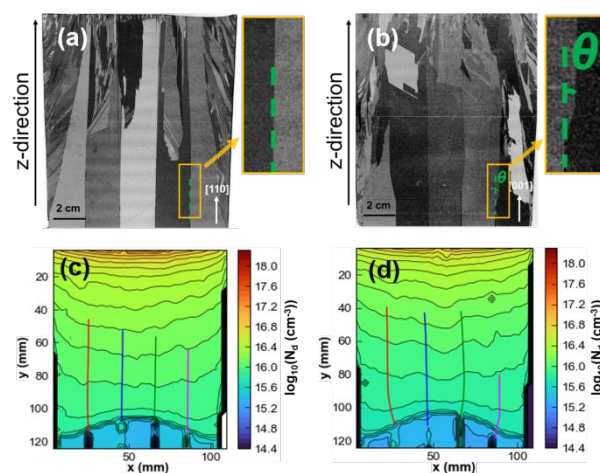


Fig. 5 The optical images of ingots cross section (a) <110>-designed GBs and (b) <100>-designed GBs. Contrast boundaries indicate GBs. Carrier concentration and the position of (c) <110>-designed GBs and (d) <100>-designed GBs. The drastic change in carrier concentration represents the boundary between the seed crystal and the growing crystal. In the initial stage of crystal growth, the solid-liquid interface is convex in the crystal growth direction.

is not known, but the average growth rate estimated from the growth time is 0.2-0.3 mm/min, which is slow enough.

### Evaluation of ingot cross-section

Wafers for evaluation were cut out of the fabricated ingots with a thickness of 1 mm at the center in the plane perpendicular to the crucible bottom and GB plane. Optical images of the as-sliced surface were taken for these wafers. By processing the optical image and extracting the line of image contrast, we identified the location of the GBs and determined their growth direction.

The solid-liquid interface shape was determined from the carrier concentration distribution measured by contact resistance measurement (four-probe method) on a longitudinal section wafer. The measurement was performed using Model RG-100PV manufactured by Napson, Inc. at a measurement interval of 2.7 mm. Contour lines of carrier density were obtained from the resistivity distribution. This contour line was assumed to be the solid-liquid interface shape.

### Results

Figures 5(a) and 5(b) show optical images of the ingot cross-section. The grains have different contrast due to the difference in seed crystal orientation. The GBs were fabricated as designed by inheriting the seed crystal orientation. In addition, we observed that crystal grains were generated from the crucible wall, but since we only evaluate the area near the residual seed crystal, it does not affect the analysis results. Figure 5(a) indicates that the <110>-designed GBs produced using the <110>-oriented seed crystal grew along the z-direction. On the other hand, Fig. 5(b) shows that the <100>-designed GBs produced using <100>-oriented seed crystal grew away from the z-direction. The random GBs, not shown here,

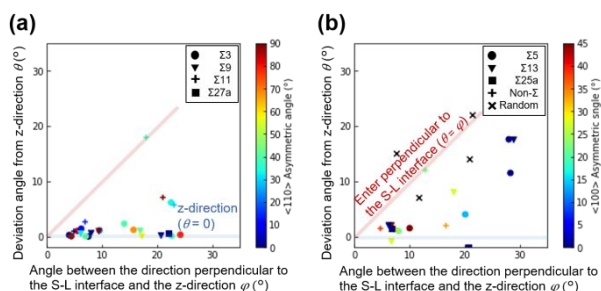


Fig. 6. Effect of the GB structure (seed crystal orientation ((a)  $\langle 110 \rangle$ -oriented, (b)  $\langle 100 \rangle$ -oriented and random) and asymmetric angle) and the initial shape of solid-liquid interface on GBs growth direction at initial stage of crystal growth.  $\theta = 0$  indicates that the GBs grow along the z-direction.  $\theta = \varphi$  indicates that the GBs grow perpendicular to the solid-liquid interface.

grew away from the z-direction as in the case of  $\langle 100 \rangle$ -designed GBs.

Figures 5(c) and 5(d) show the superimposition of artificial GBs identified by image processing on the carrier concentration distribution of the wafers shown in Figs. 5(a) and 5(b). The contour lines of the carrier concentration distribution show almost similar shapes in all ingots, which indicates that the temperature distribution during growth is highly reproducible. Therefore, the difference in the GB structures controls the growth direction of GBs instead of the different thermal histories among ingots. Due to segregation, the concentration of doping impurities in the melt changes with growth. Therefore, the contours of the carrier density reflect the shape of the growing interface. The drastic changes in the carrier concentration are seen around the bottom region to reflect the difference in doping concentration between the seed crystal and the grown crystal. This boundary corresponds to the initial position of the solid-liquid interface, and the initial shape is convex in the crystal growth direction. The solid-liquid interface shape changed from convex to concave in the crystal growth direction as the growth progressed. The GBs located at the edge of the solid-liquid interface with a large curvature tends to have a large deviation angle from the z-direction. In short, the growth direction of the GBs is affected by the solid-liquid interface shape and the GB structure (the seed crystal orientation, misorientation, asymmetric angle).

To systematically investigate the effect of the GB structure and the solid-liquid interface shape, we quantified two angle components for each of the 47 GBs. One is  $\theta$  as the deviation angle from the z-direction, and another is  $\varphi$  as the angle between the direction perpendicular to the solid-liquid interface and the z-direction. It is noted that the introduction of  $\theta$  means that a twist component is introduced although we originally designed tilt GBs.

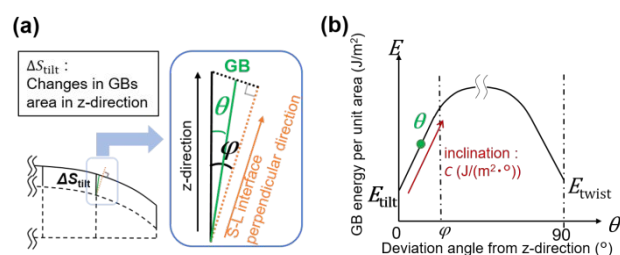


Fig. 7(a). Schematic diagram of GB growth in a short period. The green line shows the growth direction of the GB. The black arrow indicates the z-direction, and the orange arrow indicates the direction perpendicular to the solid-liquid interface. (b). Linear model assuming GBs energy per unit area. The vertical axis is the GB energy per unit area ( $E(\theta)$ ) and the horizontal axis is the deviation angle from the z-direction ( $\theta$ ). The coefficient of increase of the GB energy per unit area is expressed as  $C$ .

Figure 6 shows the effect of  $\varphi$  and the asymmetric angle ( $\beta$ ) on  $\theta$ , i.e. the GBs growth direction, for (a)  $\langle 110 \rangle$ -designed GBs and (b)  $\langle 100 \rangle$ -designed GBs, where  $\beta$  is indicated by the different color. The symbol shapes correspond to the  $\Sigma$  values of the GBs. The GBs, which do not satisfy Brandon's condition, are shown as Non- $\Sigma$ , and random GBs are shown as random. It is seen that the trend differs significantly between  $\langle 110 \rangle$ -designed GBs and  $\langle 100 \rangle$ -designed GBs, but the impact of  $\beta$  is small. For  $\langle 110 \rangle$ -designed GBs, most of the data points are located at  $\theta = 0$ . In fact, the  $\langle 110 \rangle$ -designed GBs with the  $\Sigma 3$  system ( $\Sigma 3$ ,  $\Sigma 9$ , and  $\Sigma 27a$ ) grow along the z-direction, and the  $\Sigma 11$  GBs grow slightly off the z-direction. On the other hand, for  $\langle 100 \rangle$ -designed GBs,  $\theta$  of many data points are far from 0. The  $\Sigma 5$  GBs have smaller  $\theta$  than the other  $\langle 100 \rangle$ -designed GBs. The random GBs are located along the red line with  $\theta = \varphi$ , showing that they grow almost perpendicular to the solid-liquid interface. The same trend was observed at the point where the solid-liquid interface shape was concave in the crystal growth direction. It is noted that not all the GBs follow such a trend as illustrated by the most left GB in Fig. 5(d). Such GBs are discussed in supplemental materials.

## Discussion

### Why the GB growth direction differs depending on the seed crystal orientation

The physics behind the difference in the GB growth direction would be explained by considering the impact of the GB structures on GB energies. The mechanism for determining the GB growth direction has been discussed from the viewpoint of kinetics<sup>33–35</sup>. From the viewpoint of energy, the effect of solid-liquid interface energy on the GB growth direction has been investigated using crystals with  $\langle 100 \rangle$  and  $\langle 111 \rangle$  orientations<sup>36,37</sup>. Since the crystal orientation in the z-direction is chosen as the same in this study, there is no effect of the solid-liquid interface energy. In addition, the growth rate of the ingots used in this study is slow (0.2~0.3 mm/min), and it is considered that the solid-liquid interface is not a faceted surface which is observed in high growth rate conditions. Therefore, we discuss it from the viewpoint of energy. Specifically, we consider that the GBs grow in the direction to minimize the GB energy.

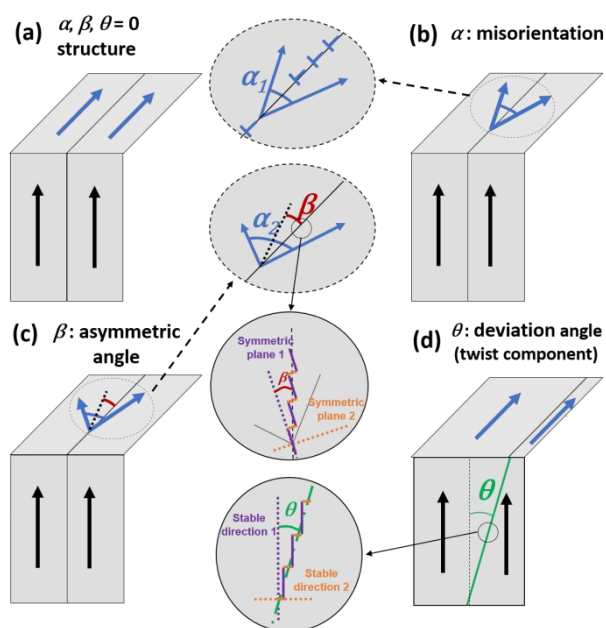


Fig. 8 Schematic diagram of the GB reconstruction mechanism with the change of  $\alpha$ ,  $\beta$ , and  $\theta$  in the case of (a)  $\alpha, \beta, \theta = 0$ , (b)  $\alpha \neq 0, \beta, \theta = 0$ , (c)  $\alpha, \beta \neq 0, \theta = 0$ , and (d)  $\alpha, \beta = 0, \theta \neq 0$ .  $\alpha$  leads to reconstruction by periodic dislocations at the grain interface.  $\beta$  results in reconstruction by forming small steps on the GB.  $\theta$  is also expected to lead to reconstruction by the formation of small steps at the GB.

Figure 7(a) shows a schematic diagram of the GB growth in a short period. The green line shows the GB with a deviation angle of  $\theta$ . GBs grow along the z-direction when  $\theta = 0$ , and they grow in the direction perpendicular to the solid-liquid interface when  $\theta = \varphi$ . The increase of the GB area in a short period,  $\Delta S(\theta)$ , can be expressed as functions of  $\theta$  and  $\varphi$  from the simple geometric relationship,

$$\Delta S(\theta) = \frac{\Delta S_{\text{tilt}} \cos \varphi}{\cos(\varphi - \theta)} \quad (1),$$

where  $\Delta S_{\text{tilt}}$  is the increase of GB area along the z-direction, i.e.,  $\theta = 0$ .

The increase of the GB energy ( $\Delta E(\theta)$ ) can be given by

$$\Delta E(\theta) = \Delta S(\theta) E(\theta) \quad (2),$$

where  $E(\theta)$  is GB energy per unit area.  $\theta$  is treated as a variable since the growth direction affects the  $\Delta S(\theta)$  and the  $E(\theta)$ . The GBs are expected to grow in the direction of  $\theta$ , which minimizes  $\Delta E$ . We assumed that  $E(\theta)$  changes as shown in Fig. 7(b). If the  $\langle 110 \rangle$ -designed GBs and  $\langle 100 \rangle$ -designed GBs grow along the z-direction ( $\theta = 0$ ), they are both tilt GBs. When the GB plane deviates from the z-direction by  $\theta$ , a twist component is introduced, resulting in mixed GBs. In this case, the larger  $\theta$  is, the more twist component is introduced. In general, the tilt and twist GBs are more stable than the mixed GBs. We assumed that  $E(\theta)$  takes the minimum  $E_{\text{tilt}}$  at  $\theta = 0$ , and increases linearly to a certain point with the introduction of the twist component because of the analogy with previous studies<sup>1,2</sup>. Figure 8 shows the schematic diagram of the GB

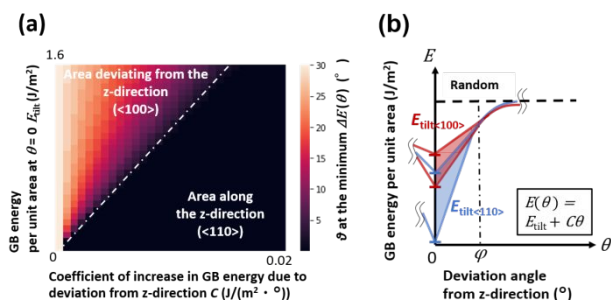


Fig. 9(a) GB growth direction calculated by assuming a linear model. The vertical axis is the GB energy per unit area ( $E_{\text{tilt}}$ ) at  $\theta = 0$ , and the horizontal axis is the coefficient of increase of the GB energy per unit area ( $C$ ) estimated by the linear model. The color map shows  $\theta$  to minimize  $\Delta E(\theta)$  when  $\varphi = 30^\circ$  (b) GB energy ( $E(\theta)$ ) per unit area for  $\langle 110 \rangle$ -designed and  $\langle 100 \rangle$ -designed GBs to explain experimental results.

reconstruction mechanism with the change of  $\alpha$ ,  $\beta$ , and  $\theta$ .  $\alpha$  leads to reconstruction by periodic dislocations at the grain interface (Fig. 8 (b)), which causes a drastic increase in the GB energy around the stable misorientation relationships<sup>2</sup>.  $\beta$  results in reconstruction by forming small steps on the GB (Fig. 8 (c)). Theoretical calculations on asymmetric tilt GBs in Al and Cu suggest that the change in GB energy with  $\beta$  is small<sup>1</sup>.  $\theta$  is also expected to lead to reconstruction by the formation of small steps at the GB (Fig. 8 (d)). However, transition to a mixed GBs (introduction of  $\theta$ ) is expected to have a larger effect on  $E(\theta)$  than the introduction of  $\beta$ , i.e., a larger slope in the energy diagram. In addition, the slope is expected to be smaller than in the case of the introduction of  $\alpha$  by analogy with the results of Ref. 1. Therefore, we assumed that  $E(\theta)$  increases linearly to a certain point with an increase of  $\theta$ . Then, from another certain point, we consider that  $E(\theta)$  decreases and reach an extreme value at  $\theta = 90^\circ$  (pure twist). Based on this theory, we simplified that  $E(\theta)$  increases linearly in the range of  $0 \leq \theta \leq \varphi$ , and can be expressed as

$$E(\theta) = E_{\text{tilt}} + C\theta \quad (3),$$

where  $C$  is a constant that indicates the slope of  $E(\theta)$  against  $\theta$  shown in Fig. 7(b). From equations (1)-(3),  $\Delta E$  can be given by

$$\Delta E(\theta) = \frac{\Delta S_{\text{tilt}} \cos \varphi}{\cos(\varphi - \theta)} (E_{\text{tilt}} + C\theta) \quad (4).$$

To minimize  $\Delta S(\theta)$ , GBs grow in the direction of  $\theta = \varphi$ . On the other hand, to minimize  $E(\theta)$ , GBs grow in the direction of  $\theta = 0$  according to Eq. (3). These suggest that  $\Delta E(\theta)$  is minimized with a certain  $\theta$  between 0 and  $\varphi$  to determine the growth direction of the GBs.

To know the GBs growth direction, the  $\theta$  that minimizes  $\Delta E(\theta)$  was obtained from Equation 4 using  $E_{\text{tilt}}$  and  $C$  as parameters ( $C: 0 \sim 0.02$ ,  $E_{\text{tilt}}: 0 \sim 1.6$ ). Figure 9(a) shows  $\theta$  to minimize  $\Delta E(\theta)$  when  $\varphi = 30^\circ$ . The black area ( $\theta = 0$ ) indicates that the GBs follow the z-direction. It is seen that  $\theta$  is larger than 0 for small  $C$  and large  $E_{\text{tilt}}$ , which means that GBs grow away from the z-direction. Fig. 9(a) shows that the GB growth direction changes continuously depending on the combination of  $E_{\text{tilt}}$  and  $C$ . In other words, the results indicated that there is a possibility that the GB may have

minimum energy in the intermediate direction. This might explain why the GBs grow not only in the z-direction or the direction perpendicular to the solid-liquid interface but also in the intermediate direction in Fig. 6(b). In addition, we revealed that the increase of  $\varphi$  leads to the increase of  $\theta$  at a given  $E_{\text{tilt}}$  and  $C$ , which also explains the experimental result.

Notably, the region with  $\theta = 0$  is found at smaller  $E_{\text{tilt}}$  and larger  $C$ , and that with  $\theta \neq 0$  is found at larger  $E_{\text{tilt}}$  and smaller  $C$ . Based on the experimental results in Fig. 6, <110>-designed GBs grew along the z-direction and <100>-designed GBs grew away from the z-direction. One possible interpretation of these results is obtained by considering  $E(\theta)$  as illustrated in Fig. 9(b).  $E_{\text{tilt}}$  is affected by  $\alpha$  and  $\beta$  and takes different values. The <100>-designed GBs are considered to form a shallow energy groove compared to the <110>-designed GBs at  $\theta = 0$ . In this case, the increase of  $E(\theta)$  with  $\theta > 0$  is overcompensated by the decrease of  $\Delta S(\theta)$  to minimize  $\Delta E(\theta)$ , and <100>-designed GBs easily grow away from the z-direction. On the other hand, <110>-designed GBs with a deep energy groove tend to grow along the z-direction ( $\theta = 0$ ) since the increase of  $\theta$  accompanies the significant increase of  $E(\theta)$ , which is not energetically favorable. This idea supports our experimental observations, where  $\Sigma 3$  system with smaller  $E_{\text{tilt}}$  took a smaller  $\theta$  than  $\Sigma 11$  GBs in <110>-designed GBs, and  $\Sigma 5$  GBs showed a smaller  $\theta$  than the other <100>-designed GBs.  $E_{\text{tilt}}$  for low- $\Sigma$  GBs have been calculated for several structures, and the order of  $E_{\text{tilt}}$  classified by  $\Sigma$  values are consistent with our ideas<sup>2,6,38–43</sup> (Table 1 of the supplemental materials describes the GB structure,  $E_{\text{tilt}}$  and GB behavior in our experiment). In addition, as we described above, theoretical calculations on asymmetric tilt GBs in Al and Cu suggest that the change in GB energy with  $\beta$  is small<sup>1</sup>. This supports our consideration that the effect of  $\beta$  on the  $E_{\text{tilt}}$  is small.

Finally, we consider random GBs and  $\{112\}\Sigma 3$  GBs. Since random GBs do not have a specific stable crystallographic orientation relationship,  $E(\theta)$  is regarded as a constant. In this case, our theory suggests that the growth direction is perpendicular to the solid-liquid interface since  $\Delta E(\theta)$  is minimized by minimizing  $\Delta S(\theta)$ . This prediction is in good agreement with the experimental observation reported by Prakash *et al.*<sup>28</sup>. As for  $\{112\}\Sigma 3$  GBs,  $E_{\text{tilt}}$  is quite small and <110> orientation can be the growth direction. In this case, the GB is considered to grow along the z-direction controlled by the minimization of  $E(\theta)$ . This is supported by the experimental observation reported by Chuang *et al.*<sup>29</sup>. As illustrated by these examples, our theory could explain various experimental observations of the growth direction of GBs.

## Conclusions

The effect of the GB structure on the growth direction was systematically investigated using asymmetric GBs obtained using purposely designed seed crystals. We found that the seed crystal orientation has a significant effect on the growth direction of the GB, while the asymmetric angle has little effect. The <110>-designed GBs grew along the z-direction, while <100>-designed GBs grew away from the z-direction. We explained these phenomena based on a simple linear model of the GB energy per unit area and found that GBs with shallow energy grooves are more likely to grow

away from the z-direction like <100>-designed GBs. This suggests that the growth of <100>-designed GBs requires more strict control of the solid-liquid interface shape to control the growth direction. As illustrated by this example, we should establish a control method depending on the structure of GBs. This discipline is not limited to multicrystalline silicon, and the appropriate controlling method that matches the GB structure should be developed to realize polycrystalline materials with controlled GBs and better functions.

## Author Contributions

Yusuke Fukuda: Methodology, Formal analysis, Investigation, Data Curation, Writing - Original Draft, Kentaro Kutsukake: Conceptualization, Methodology, Investigation, Validation, Writing - Review & Editing, Takuto Kojima: Formal analysis, Software, Validation, Noritaka Usami: Conceptualization, Writing - Review & Editing, Supervision, Funding acquisition

## Conflicts of interest

There are no conflicts to declare.

## Acknowledgments

This work was partly supported by JST/CREST, Grant No. JPMJCR17J1 (2017-2023).

## References

- 1 M. A. Tschopp and D. L. McDowell, *Philosophical Magazine*, 2007, **87**, 3871–3892.
- 2 M. Kohyama, R. Yamamoto and M. Doyama, *Physica Status Solidi B-basic Solid State Physics*, 1986, **138**, 387.
- 3 J. Chen and T. Sekiguchi, *Japanese Journal of Applied Physics, Part 1: Regular Papers and Short Notes and Review Papers*, 2007, **46**, 6489–6497.
- 4 Y. Ohno, T. Tamaoka, H. Yoshida, Y. Shimizu, K. Kutsukake, Y. Nagai and N. Usami, *Applied Physics Express*, 2021, **14**, 011002.
- 5 M. Kohyama and R. Yamamoto, *Physical Review B*, 1994, **50**, 8502–8522.
- 6 M. Kohyama, R. Yamamoto, Y. Ebata and M. Kinoshita, *Journal of Physics C: Solid State Physics*, 1988, **21**, 3205–3215.

Journal Name	ARTICLE
7 R. Shimokawa and Y. Hayashi, <i>Journal of Applied Physics</i> , 1986, <b>59</b> , 2571–2576.	21 K. Kutsukake, N. Usami, K. Fujiwara, Y. Nose and K. Nakajima, <i>Journal of Applied Physics</i> , 2007, <b>101</b> , 063509.
8 X. Wang, X. Song, H. Wang, X. Liu, X. Liu and G. Guo, <i>CrystEngComm</i> , 2016, <b>18</b> , 471–479.	22 Z.-J. Wang and T. Watanabe, <i>Interface Science</i> , 1999, <b>7</b> , 197–205.
9 A. Senthamizhan, B. Balusamy, Z. Aytac and T. Uyar, <i>CrystEngComm</i> , 2016, <b>18</b> , 6341–6351.	23 A. Bary and G. Nouet, <i>Journal of Applied Physics</i> , 1988, <b>63</b> , 435–438.
10 A. Ravi Shankar, V. Shankar, R. P. George and J. Philip, <i>Corrosion</i> , 2020, <b>76</b> , 835–842.	24 N. Usami, M. Kitamura, T. Sugawara, K. Kutsukake, K. Ohdaira, Y. Nose, K. Fujiwara, T. Shishido and K. Nakajima, <i>Japanese Journal of Applied Physics</i> , 2005, <b>44</b> , 778–780.
11 T. Liu, S. Xia, Q. Bai, B. Zhou, Y. Lu and T. Shoji, <i>Materials</i> , 2019, <b>12</b> (2), 242.	25 K. Kutsukake, N. Usami, T. Ohtaniuchi, K. Fujiwara and K. Nakajima, <i>Journal of Applied Physics</i> , 2009, <b>105</b> , 044909.
12 H. Yoshida, K. Okada, Y. Ikuhara and T. Sakuma, <i>Philosophical Magazine Letters</i> , 1997, <b>76</b> , 9–14.	26 H. Y. Wang, N. Usami, K. Fujiwara, K. Kutsukake and K. Nakajima, <i>Acta Materialia</i> , 2009, <b>57</b> , 3268–3276.
13 H. Yoshida, Y. Ikuhara and T. Sakuma, <i>Acta Materialia</i> , 2002, <b>50</b> , 2955–2966.	27 T. Yokoi, Y. Noda, A. Nakamura and K. Matsunaga, <i>Physical Review Materials</i> , 2020, <b>4</b> , 014605.
14 H. Yoshida, Y. Ikuhara, T. Sakuma, M. Sakurai and E. Matsubara, <i>Philosophical Magazine</i> , 2004, <b>84</b> , 865–876.	28 R. R. Prakash, T. Sekiguchi, K. Jiptner, Y. Miyamura, J. Chen, H. Harada and K. Kakimoto, <i>Journal of Crystal Growth</i> , 2014, <b>401</b> , 717–719.
15 F. Zhang, X. Yu, C. Liu, S. Yuan, X. Zhu, Z. Zhang, L. Huang, Q. Lei, D. Hu and D. Yang, <i>Solar Energy Materials and Solar Cells</i> , 2019, <b>200</b> , 109985.	29 L. C. Chuang, K. Maeda, K. Shiga, H. Morito and K. Fujiwara, <i>Scripta Materialia</i> , 2019, <b>167</b> , 46–50.
16 K. Kutsukake, N. Usami, Y. Ohno, Y. Tokumoto and I. Yonenaga, <i>Applied Physics Express</i> , 2013, <b>6</b> , 025505.	30 K. Kutsukake, N. Usami, K. Fujiwara, Y. Nose, T. Sugawara, T. Shishido and K. Nakajima, <i>Materials Transactions</i> , 2007, <b>48</b> , 143–147.
17 K. Kutsukake, N. Usami, Y. Ohno, Y. Tokumoto and I. Yonenaga, <i>IEEE Journal of Photovoltaics</i> , 2014, <b>4</b> , 84–87.	31 T. Iwata, I. Takahashi and N. Usami, <i>Japanese Journal of Applied Physics</i> , 2017, <b>56</b> , 075501.
18 A. K. Fedotov, A. V. Mazanik, E. A. Katz, Yu. Ilyashuk, A. Drozdovski and L. E. Polyak, <i>Solid State Phenomena</i> , 1999, <b>67–68</b> , 15–20.	32 I. Takahashi, N. Usami, K. Kutsukake, G. Stokkan, K. Morishita and K. Nakajima, <i>Journal of Crystal Growth</i> , 2010, <b>312</b> , 897–901.
19 M. G. Tsoutsouva, P. E. Vullum, K. Adamczyk, M. di Sabatino and G. Stokkan, <i>Journal of Applied Physics</i> , 2020, <b>127</b> , 125109.	33 T. Duffar and A. Nadri, <i>Comptes Rendus Physique</i> , 2013, <b>14</b> , 185–191.
20 S. Tsurekawa, K. Kido, S. Hamada, T. Sekiguchi, <i>Zeitschrift fuer Metallkunde</i> , 2005, <b>96</b> , 197–206.	

## ARTICLE

## Journal Name

- 34 K. Fujiwara, S. Tsumura, M. Tokairin, K. Kutsukake, N. Usami, S. Uda and K. Nakajima, *Journal of Crystal Growth*, 2009, **312**, 19–23.
- 35 K. K. Hu, K. Maeda, H. Morito, K. Shiga and K. Fujiwara, *Acta Materialia*, 2018, **153**, 186–192.
- 36 K. Fujiwara, Y. Obinata, T. Tujihara, N. Usami, G. Sazaki and K. Nakajima, *Journal of Crystal Growth*, 2004, **262**, 124–129.
- 37 K. Fujiwara, Y. Obinata, T. Tujihara, N. Usami, G. Sazaki and K. Nakajima, *Journal of Crystal Growth*, 2004, **266**, 441–448.
- 38 L. F. Mattheiss and J. R. Patel, *Physical Review B*, 1981, **23**, 5384–5396.
- 39 M. Kohyama, R. Yamamoto and M. Doyama, *Physica Status Solidi B-basic Solid State Physics*, 1986, **137**, 11.
- 40 R. E. Thomson and D. J. Chadi, *Physical Review B*, 1984, **29**, 889–892.
- 41 D. P. DiVincenzo, O. L. Alerhand, M. Schlüter and J. W. Wilkins, *Physical Review Letters*, 1986, **56**, 1925–1928.
- 42 J. Hornstra, *Physica*, 1960, **26**, 198–208.
- 43 F. H. Stillinger and T. A. Weber, *Physical Review B*, 1985, **31**, 5262–5271.